ACS APPLIED MATERIALS & INTERFACES

Research Article

www.acsami.org

Effects of Alkyl Chain Length and Substituent Pattern of Fullerene Bis-Adducts on Film Structures and Photovoltaic Properties of Bulk Heterojunction Solar Cells

Ran Tao,[†] Tomokazu Umeyama,[†] Kei Kurotobi,[‡] and Hiroshi Imahori*[,†,‡]

[†]Department of Molecular Engineering, Graduate School of Engineering, and [‡]Institute for Integrated Cell-Material Sciences (WPI-iCeMS), Kyoto University, Nishikyo-ku, Kyoto 615-8510, Japan

Supporting Information

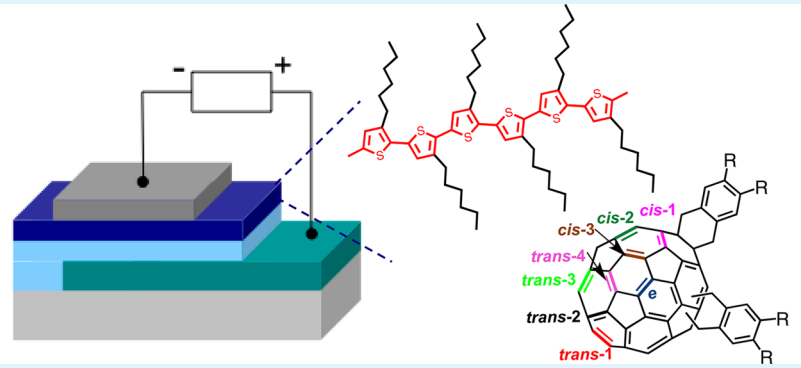

ABSTRACT: A series of alkoxycarbonyl-substituted dihydronaphthyl-based [60]fullerene bis-adduct derivatives (denoted as C2BA, C4BA, and C6BA with the alkyl chain of ethyl, *n*-butyl, and *n*-hexyl, respectively) have been synthesized to investigate the effects of alkyl chain length and substituent pattern of fullerene bis-adducts on the film structures and photovoltaic properties of bulk heterojunction polymer solar cells. The shorter alkyl chain length caused lower solubility of the fullerene bis-adducts (C6BA > C4BA > C2BA), thereby resulting in the increased separation difficulty of respective bis-adduct isomers. The device performance based on poly(3-hexylthiophene) (P3HT) and the fullerene bis-adduct regioisomer mixtures was enhanced by shortening the alkyl chain length. When using the regioisomerically separated fullerene bis-adducts, the devices based on *trans*-2 and a mixture of *trans*-4 and *e* of C4BA exhibited the highest power conversion efficiencies of ca. 2.4%, which are considerably higher than those of the C6BA counterparts (ca. 1.4%) and the C4BA regioisomer mixture (1.10%). The film morphologies as well as electron mobilities of the P3HT:bis-adduct blend films were found to affect the photovoltaic properties considerably. These results reveal that the alkyl chain length and substituent pattern of fullerene bis-adducts significantly influence the photovoltaic properties as well as the film structures of bulk heterojunction solar cells.

KEYWORDS: *polymer solar cell, fullerene, regioisomer, alky chain length, bulk heterojunction*

INTRODUCTION

In the past decade, polymer solar cells (PSCs) as one of the most potential renewable energy technologies have undergone tremendous development due to their advantages of low cost, light weight, and large-area processability.[1−6] The most successful PSC devices to date are based on a bulk heterojunction (BHJ) structure, which typically has an interpenetrating bicontinuous network comprised of electron-donating conjugated polymers and electron-accepting fullerene monoadduct derivatives. The past decade has witnessed a rapid increase in the power conversion efficiencies (PCEs), exceeding 9% in single BHJ PSCs.[7]

The PCE value of PSCs is determined by three factors: short-circuit current density (J_{SC}), open-circuit potential (V_{OC}), and fill factor (FF). Among these, V_{OC} value is mainly proportional to the energy difference between the highest occupied molecular orbital (HOMO) of the donor and the lowest unoccupied molecular orbital (LUMO) of the acceptor.[8,9] At the molecular level, lowering the HOMO level of electron-donating conjugated polymers, raising the LUMO level of electron-accepting fullerene derivatives, or both could lead to a larger V_{OC} value. However, lowering a polymer's HOMO level inevitably increases its optical bandgap and thereby sacrifices its J_{SC} value owing to the depleted light-harvesting ability of the polymer as a major sensitizer. On the other hand, bis- and multiadducts of fullerenes are known to possess up-shifted LUMO levels compared to their corresponding monoadducts, enhancing the V_{OC} and PCE values of PSCs.[10−28] The second

Received: August 30, 2014
Accepted: September 10, 2014
Published: September 10, 2014

functionalization on the fullerene framework of the monoadduct further reduces the π-conjugation as well as electron delocalization in the fullerene. This electronic alternation in the bis-adduct makes the first one-electron reduction potential more negative, yielding the higher-lying LUMO level. For instance, the LUMO level of a typical fullerene acceptor [60]PCBM ([6,6]-phenyl-C_{61}-butyric acid methyl ester) can be elevated by 0.1 eV by covalently tethering the same substituent to [60]PCBM, resulting in a 20% increase in V_{OC} and PCE.[10,11] Meanwhile, a tris-adduct of [60]PCBM yielded a lower PCE irrespective of an additional increase of 0.1 eV for the LUMO level.[11,29] The insulating addends that surround the fullerene core more intensively would inversely cause a reduction of electron mobility originating from unfavorable loose packing of the fullerene cores interrupted by the addends.

Despite successful application of fullerene bis-adducts to PSCs, their regioisomer mixtures have been directly used without separating each isomer. Inherently, [60]fullerene bis-adducts with symmetrical substituents have eight regioisomers: *trans*-1, *trans*-2, *trans*-3, *trans*-4, *e*, *cis*-1, *cis*-2, and *cis*-3 (Figure 1). Aside from a few exception,[30] the current synthetic routes to

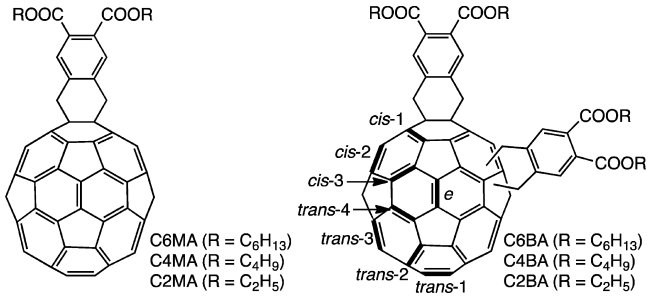

Figure 1. Structures of fullerene monoadducts, bis-adducts, and their isomers.

fullerene bis-adducts invariably generate a mixture of regioisomers, and the isomer ratio and distribution in the fullerene bis-adduct mixture are highly dependent on synthetic conditions such as temperature, reaction time, and concentration of the reactants.[31] Given that molecular packing and arrangement of fullerene acceptors in the BHJ structure have a large influence on charge separation and electron-transporting processes, a pure bis-adduct isomer with two addends at specific positions on C_{60} would yield a more desirable network in the active layer, leading to a better device performance. Accordingly, it is extremely pivotal to elucidate the close relationship between the molecular structure of [60]fullerene bis-adduct regioisomers and photovoltaic performance.

Recently, we have conducted the regioisomer separation of hexyloxycarbonyl-substituted dihydronaphthyl-based [60]-fullerene bis-adducts (C6BA, Figure 1) and applied the separated bis-adducts to PSCs for the first time.[22] To reduce the plausible number of the fullerene bis-adduct isomers, a symmetrical dihydronaphthyl group was chosen as the substituent. We expected that symmetrical introduction of two long alkoxycarbonyl chains into the dihydronaphthyl groups would facilitate the isomer separation and purification. Indeed, repeated separations by HPLC equipped with a Buckyprep column afforded *trans*-1, *trans*-2, *trans*-3, *trans*-4, *e*, and a mixture of *cis*-2 and *cis*-3 (denoted as *cis*-2+*cis*-3) isomers. The LUMO energy levels of C6BA isomers estimated by cyclic voltammetry are 0.1−0.2 eV higher than those of the corresponding monoadduct (C6MA, Figure 1) and [60]PCBM. However, the best PCE (1.44%) achieved by the *trans*-4 isomer of C6BA (denoted as C6BA−*trans*-4) in combination with regioregular poly(3-hexylthiophene) (P3HT) was lower than those of the corresponding monoadduct C6MA and [60]PCBM-based PSCs (1.71 and 2.10%, respectively).[22] The inferior efficiencies may be caused by the long aliphatic side chains, which disrupt the optimal packing and efficient electron transport of the fullerene molecules in the active layer.[32,33] Hence, we decided to shorten the *n*-hexyl chain of C6BA to *n*-butyl and ethyl (C4BA and C2BA, Figure 1). We expected that we could systematically address the effects of alkyl chain length as well as substituent pattern of fullerene bis-adducts on the photovoltaic properties of PSCs. Furthermore, the relationship between PSC device performances and nanostructured phase separations in the active layer is also discussed.

EXPERIMENTAL SECTION

Instruments. Fullerene bis-adduct isomers separation was accomplished by Japan Analytical Industry LC-908 with Nacalai Tesque Cosmosil buckyprep. ^{1}H NMR and ^{13}C NMR spectra were measured with a JEOL JNM-EX400 NMR spectrometer. High-resolution mass spectra were measured on a JEOL JMS-700 MStation spectrometer (ESI). Attenuated total reflectance (ATR) FT-IR spectra were recorded on a ThermoFisher Scientific Nicolet 6700 FT-IR. UV−vis absorption spectra were obtained on a PerkinElmer Lambda 900 UV/vis/NIR spectrometer. Photoluminescence (PL) spectra were recorded with a HORIBA SPEX Fluoromax-3 spectrofluorometer. Atomic force microscopy (AFM) analyses were carried out with an Asylum Technology MFP-3D-SA in ac mode. X-ray diffraction (XRD) analyses were carried out in a Rigaku SmartLab 9 kW using Cu Kα radiation. Thermogravimetric analysis (TGA) measurements were conducted with a SHIMADZU DTG-60 under flowing nitrogen at a scan rate of 10 °C min^{-1}. Differential scanning calorimetry (DSC) analysis was made on a SHIMAZU DSC-60 under flowing nitrogen at a scan rate of 10 °C min^{-1}. Cyclic voltammetry (CV) and differential pulse voltammetry (DPV) measurements were performed using an ALS 630A electrochemical analyzer in *o*-dichlorobenzene (ODCB)/acetonitrile mixture (v:v = 5:1) containing 0.1 M tetrabutylammonium hexafluorophosphate (Bu_4PF_6) as a supporting electrolyte. Photocurrent−voltage characteristics were measured by PECK2400-N with PEC-L11 solar simulator (Peccell Technologies) under standard two-electrode conditions (100 mW cm^{-2}, AM1.5). Photocurrent action spectra were recorded with CEP-2000RR (Bunkoukeiki). Current−voltage characteristics of the electron-only devices for space-charge-limited current (SCLC) measurements were conducted using a Keithley 4200-SCS characterization system under an argon atmosphere.

Materials. C_{60} (99.98%) was obtained from MTR Ltd. and used as-received. All other solvents and chemicals were of reagent-grade quality, purchased commercially, and used without further purification unless otherwise noted. Thin layer chromatography (TLC) and column chromatography were performed with Silica gel 60 F_{254} (Merck) and SiliaFlash F60 (230−400 mesh; SiliCycle Inc.), respectively. 4,5-Bis(methoxycarbonyl)benzocyclobutene (R1), 4,5-bis(hexyloxycarbonyl)benzocyclobutene (R2), and C6BA were prepared according to the reported procedures.[22,34]

Synthesis. 4,5-Bis(butoxycarbonyl)benzocyclobutene (R3): R1 (1.43 g, 6.5 mmol), *n*-butanol (5.95 mL, 65 mmol), and sulfuric acid (0.15 mL) were dissolved in toluene (9 mL) under argon atmosphere, and then the solution was refluxed for 44 h. The reaction mixture was washed with saturated $NaHCO_3$ solution, water, and saturated NaCl solution and dried over anhydrous Na_2SO_4 and evaporated. Purification by column chromatography on silica gel using mixed solvent (hexane:ethyl acetate = 5:1) as eluent yielded R3 (1.68 g, 85%) as colorless oil. ^{1}H NMR ($CDCl_3$, 400 MHz): δ 7.38 (s, 2H), 4.28 (m, 4H), 3.23 (s, 4H), 1.73 (m, 4H), 1.44 (m, 4H), 0.96 (m, 6H).

IR (ATR): ν_{max}/cm^{-1} 2959, 2873, 1719, 1587, 1463, 1384, 1336, 1252, 1189, 1099, 1062, 1018, 943, 891, 842, 780, 738. HRMS (ESI): calcd for $C_{18}H_{24}O_4$[M + H] 305.1747, found 305.1745.

C4BA: R3 (1.36 g, 4.5 mmol) and C_{60} (1.61 g, 2.2 mmol) were dissolved in ODCB (150 mL), and then the solution was refluxed for 96 h under argon atmosphere. Subsequently, the reaction mixture was evaporated. The unreacted C_{60}, the corresponding monoadduct (C4MA, Figure 1), and C4BA were separated from the reaction mixture by silica gel column chromatography with toluene and CH_2Cl_2. Then, C4BA was further purified by preparative HPLC with toluene. A total of 1.67 g of C4BA as a regioisomer mixture was obtained (yield 57%). ^{1}H NMR ($CDCl_3$, 400 MHz): δ 8.30−7.74 (m, 4H), 5.06−4.05 (m, 16H), 1.92−1.66 (m, 8H), 1.51−1.38 (m, 8H), 1.08−0.91 (m, 12H). IR (ATR): ν_{max}/cm^{-1} 2954, 2924, 2866, 1716, 1617, 1570, 1454, 1415, 1381, 1329, 1277, 1216, 1165, 1117, 1057, 1031, 959, 940, 898, 843, 786, 749, 695. HRMS (ESI): calcd for $C_{96}H_{48}O_8$[M + H] 1329.3427, found 1329.3429.

R4. A solution of 1,5-hexadiyne (0.92 g, 11.8 mmol) and diethyl acetylenedicarboxylate (1.35 g, 8 mmol) in 1:1.5 *n*-octane/toluene (total volume 25 mL) was added slowly by syringe pump (addition time: 6 h) to a refluxing solution of $CpCo(CO)_2$ (0.2 mL) in *n*-octane (24 mL) under argon atmosphere. The reaction mixture was refluxed for 18 h at 130 °C under N_2. Then, the reaction mixture was cooled to room temperature, evaporated, and purified by column chromatography. Elution of the column with mixed solvent (hexane:ethyl acetate 2:1) gave the desired product R4 as colorless oil (0.87 g, 61%). ^{1}H NMR ($CDCl_3$, 400 MHz): δ 7.39 (s, 2H), 4.33 (m, 4H), 3.23 (s, 4H), 1.36 (t, 6H). IR (ATR): ν_{max}/cm^{-1} 2981, 2936, 1716, 1585, 1463, 1389, 1368, 1334, 1251, 1190, 1099, 1020, 896, 866, 780. HRMS (ESI): calcd for $C_{14}H_{16}O_4$[M + H] 249.1121, found 249.1122.

C2BA: R4 (1.37 g, 5.5 mmol) and C_{60} (1.99 g, 2.8 mmol) were dissolved in ODCB (150 mL), and then the solution was refluxed for 62 h under argon atmosphere. Subsequently, the solvents of the reaction mixture were removed. The unreacted C_{60}, the corresponding monoadduct (C2MA, Figure 1), and C2BA were separated from the reaction mixture by silica gel column chromatography with toluene and CH_2Cl_2. Then, C2BA was further purified by preparative HPLC with toluene. A total 1.73 g of C2BA as a regioisomer mixture was obtained (yield 51%). ^{1}H NMR ($CDCl_3$, 400 MHz): δ 8.25−7.75 (m, 4H), 5.05−4.05 (m, 16H), 1.52−1.32 (m, 12H). IR (ATR): ν_{max}/cm^{-1} 2976, 2936, 2908, 1714, 1614, 1570, 1442, 1413, 1365, 1328, 1260, 1217, 1200, 1168, 1115, 1016, 969, 900, 854, 761, 729, 693. HRMS (ESI): calcd for $C_{88}H_{32}O_8$[M + Na] 1239.1995, found 1239.1972.

Separation and Purification of C4BA Isomers. Separation and purification were accomplished with a Buckyprep column at 50 °C.

trans-1 Isomer. ^{1}H NMR ($C_2D_2Cl_4$, 5.91, 400 MHz): δ 8.06 (s, 4H), 4.87 (s, 4H), 4.38 (t, 8H), 1.83−1.76 (m, 8H), 1.52−1.47 (m, 8H), 0.99 (t, 12H). ^{13}C NMR ($C_2D_2Cl_4$, 73.78, 393 K, 400 MHz): δ 167.27, 154.48, 147.85, 145.26, 145.15, 144.23, 141.96, 141.26, 140.82, 136.04, 132.22, 128.31, 65.60, 63.28, 44.69, 30.61, 19.06, 13.45. IR (ATR): ν_{max}/cm^{-1} 2957, 2922, 2868, 1717, 1616, 1572, 1455, 1428, 1392, 1331, 1279, 1220, 1197, 1170, 1123, 1061, 1048, 1035, 956, 898, 761, 733, 691. HRMS (ESI): calcd for $C_{96}H_{48}O_8$[M + H] 1329.3427, found 1329.3424.

trans-2 Isomer. ^{1}H NMR ($C_2D_2Cl_4$, 5.91, 400 MHz): δ 8.04 (s, 2H), 7.97 (s, 2H), 4.80 (d, 2H), 4.62 (d, 4H), 4.51 (d, 2H), 4.39−4.34 (m, 8H), 1.81−1.74 (m, 8H), 1.52−1.45 (m, 8H), 1.01−0.96 (m, 12H). ^{13}C NMR ($C_2D_2Cl_4$, 73.78, 393 K, 400 MHz): δ 167.37, 154.36, 154.20, 153.76, 147.74, 147.14, 146.96, 146.73, 146.68, 146.17, 145.66, 145.50, 145.26, 144.80, 144.25, 144.09, 143.64, 142.77, 142.56, 142.53, 142.11, 141.47, 141.25, 141.13, 139.81, 139.32, 134.08, 133.06, 132.24, 128.92, 128.40, 128.35, 128.10, 65.57, 64.43, 64.19, 44.95, 43.62, 30.54, 30.47, 18.98, 18.93, 13.39, 13.34. IR (ATR): ν_{max}/cm^{-1} 2954, 2925, 2870, 1716, 1618, 1570, 1454, 1430, 1412, 1381, 1328, 1267, 1218, 1201, 1165, 1117, 1060, 1034, 941, 899, 841, 766, 733, 715, 693. HRMS (ESI): calcd for $C_{96}H_{48}O_8$[M + H] 1329.3427, found 1329.3431.

trans-3 Isomer. ^{1}H NMR ($C_2D_2Cl_4$, 5.91, 400 MHz): δ8.01 (s, 2H), 7.78 (s, 2H), 4.65 (d, 2H), 4.56 (d, 2H), 4.38−4.27 (m, 12H), 1.80−1.69 (m, 8H), 1.52−1.41 (m, 8H), 1.01−0.93 (m, 12H). ^{13}C NMR ($C_2D_2Cl_4$, 73.78, 393 K, 400 MHz): 167.32, 167.30, 159.57, 156.87, 156.81, 155.73, 149.36, 149.24, 148.58, 148.34, 148.11 145.74, 145.40, 145.37, 145.29, 144.75, 144.07, 143.86, 143.68, 142.80, 141.65, 141.40, 141.27, 141.03, 140.90, 139.65, 136.03, 134.81, 132.13, 132.08, 128.29, 128.14, 65.57, 65.51, 64.43, 64.19, 44.95, 43.62, 30.54, 30.47, 18.98, 18.93, 13.39, 13.34. IR (ATR): ν_{max}/cm^{-1} 2954, 2931, 2867, 1710, 1618, 1570, 1454, 1330, 1264, 1215, 1167, 1119, 1061, 1031, 941, 897, 845, 736, 708, 694. HRMS (ESI): calcd for $C_{96}H_{48}O_8$[M + H] 1329.3427, found 1329.3435.

trans-4 and e Isomers (Mixture). ^{1}H NMR ($C_2D_2Cl_4$, 5.91, 400 MHz): δ 7.88−7.75 (m, 4H), 4.42−4.22 (m, 16H), 1.77−1.70 (m, 8H), 1.49−1.38 (m, 8H), 0.99−0.93 (m, 12H). ^{13}C NMR ($C_2D_2Cl_4$, 73.78, 393 K, 400 MHz): δ 167.31, 167.17, 160.78, 155.51, 154.56, 154.22, 153.76, 151.98, 151.39, 151.31, 150.26, 149.41, 149.09, 148.09, 148.00, 147.29, 147.26, 146.91, 146.42, 146.20, 146.15, 145.97, 145.84, 145.74, 145.59, 145.10, 144.99, 144.68, 144.57, 144.55, 144.44, 144.01, 143.81, 142.88, 142.72, 142.21, 142.06, 141.90, 141.76, 141.66, 141.19, 141.03, 140.97, 140.90, 140.70, 140.58, 140.47, 138.81, 137.28, 136.34, 134.60, 132.48, 132.00, 131.97, 131.87, 131.79, 130.39, 128.09, 128.01, 127.95, 127.54, 65.61, 65.56, 65.53, 64.08, 63.95, 63.82, 63.73, 63.59, 44.69, 44.60, 44.56, 44.44, 44.28, 43.51, 30.55, 30.48, 23.98, 23.22, 19.04, 19.01, 19.00, 13.46. IR (ATR): ν_{max}/cm^{-1} 2947, 2924, 2856, 1715, 1618, 1572, 1453, 1414, 1380, 1330, 1265, 1216, 1198, 1161, 1060, 1032, 947, 904, 844, 767, 742, 695. HRMS (ESI): calcd for $C_{96}H_{48}O_8$[M + H] 1329.3427, found 1329.3443.

cis-2 and cis-3 Isomers (Mixture). ^{1}H NMR ($C_2D_2Cl_4$, 5.91, 400 MHz): δ 7.78 (s, 2H), 7.76 (s, 2H), 4.34−3.91 (m, 16H), 1.77−1.70 (m, 8H), 1.49−1.42 (m, 8H), 0.98−0.93 (m, 12H). ^{13}C NMR ($C_2D_2Cl_4$, 73.78, 393 K, 400 MHz): δ 167.30, 167.28, 167.25, 167.19, 167.07, 160.12, 157.69, 157.67, 154.57, 153.05, 150.36, 149.50, 149.43, 148.89, 148.57, 148.23, 147.73, 147.59, 147.35, 147.05, 146.94, 146.79, 146.44, 146.33, 146.04, 145.88, 145.74, 145.44, 145.29, 145.02, 144.77, 144.58, 144.55, 144.46, 144.24, 142.67, 142.10, 142.08, 141.81, 141.67, 141.48, 141.17, 141.05, 140.97, 140.74, 140.29, 138.51, 137.63, 133.37, 132.08, 132.03, 131.93, 128.92, 128.88, 128.42, 128.41, 128.24, 128.05, 128.01, 127.54, 65.67, 65.61, 65.54, 65.49, 65.46, 65.42, 65.37, 64.10, 63.93, 62.54, 61.47, 60.15, 44.52, 42.84, 42.81, 30.56, 30.41, 30.38, 19.04, 19.00, 18.90, 13.44. IR (ATR): ν_{max}/cm^{-1} 2949, 2868, 1715, 1615, 1570, 1454, 1414, 1384, 1328, 1272, 1215, 1167, 1116, 1059, 1030, 941, 842, 786, 744, 690. HRMS (ESI): calcd for $C_{96}H_{48}O_8$[M + H] 1329.3427, found 1329.3439.

Quantum Chemical Calculation. Geometry optimization and electronic structure calculations for the fullerene compounds were performed using density functional theory (DFT) at the RB3LYP/6-31G (d) level. The calculations were carried out with Gaussian 03 software package using a spin-restricted formalism.[35] The electron density diagrams of molecular orbitals were obtained with the ChemBioOffice 2010 graphics program.

Device Fabrication. The organic solar cells were fabricated as follows.[36−39] An indium tin oxide (ITO) glass substrate with a sheet resistance of 5 Ω/sq (Geomatec) was used. The substrates were sonicated consecutively with detergent, deionized water, 2-propanol, and ethanol for 15 min. After being dried and UV-ozone treated, the substrates were spin-coated with poly(ethylene dioxythiophene) doped with poly(styrene sulfonic acid) (PEDOT:PSS, Clevios P VP AI 4083) at 1000 rpm and dried at 200 °C for 10 min. Afterward, a mixed solution of P3HT (15 mg mL^{-1}) and fullerene derivative (13.5 mg mL^{-1} for C6BA mixtures, C6BA regioisomers, C4BA mixtures, C2BA mixtures, and [60]PCBM (American Dye Source, Inc.) and 10.5 mg mL^{-1} for C4BA regioisomers) in ODCB was spin-coated at 1500 rpm for 1 min onto the PEDOT:PSS layer under an argon atmosphere. The P3HT:fullerene blend film had a thickness of ca. 90 nm. Then, 100 nm Al cathode was further deposited onto the active layer to yield the layered device structure (denoted as ITO/PEDOT:PSS/P3HT:fullerene/Al). The device was post-thermal annealed at 150 °C for 15 min. Schematic illustrations of the top and side views of the device are depicted in Figure S1 (see Supporting Information). The size of each device was 0.06 cm^2 (0.2 × 0.3 cm^2). For the device based on the P3HT:[60]PCBM film exhibiting a maximum PCE value, we used a mixed solution of P3HT (13.6 mg

Scheme 1. Synthetic Routes to Fullerene Bis-Adducts

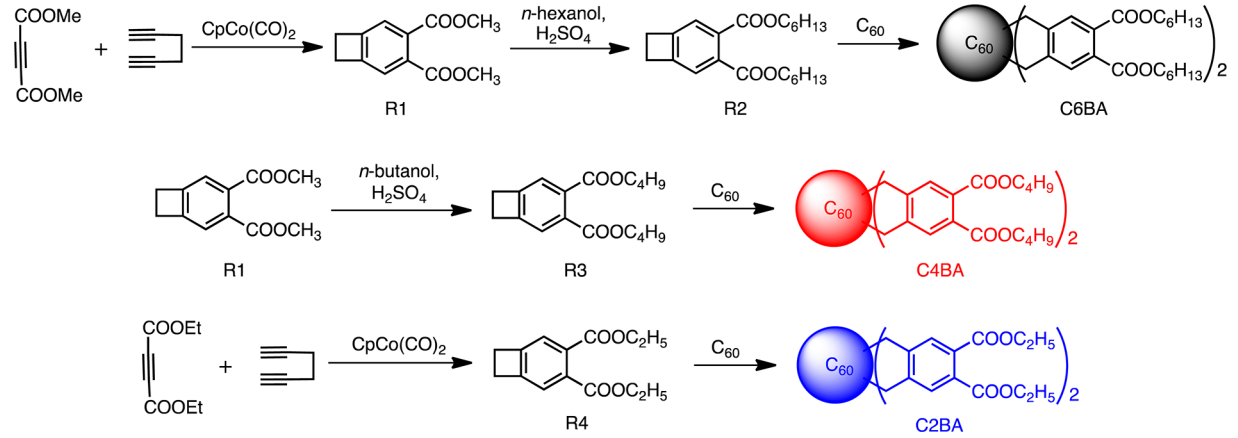

mL^{-1}) and [60]PCBM (8.2 mg mL^{-1}) in chlorobenzene and spin-coated it at 1000 rpm for 30 s and then 2000 rpm for 10 s. In addition, postannealing was conducted at 150 °C for 6 min.

The electron-only devices were fabricated as follows. A 50 nm aluminum film was first thermally deposited onto the glass substrate. The P3HT:fullerene blend film with a thickness of 150−200 nm was spin-coated at 700 rpm for 2 min. Then, the active layer was capped by a 100 nm aluminum electrode.

RESULTS AND DISCUSSION

Synthesis and Isolation. The synthetic route to the C4BA regioisomer mixture is similar to the published method for C6BA[22] as outlined in Scheme 1. Ester-exchange reaction of benzocyclobutene R1 with *n*-butanol afforded the precursor compound R3 for *o*-quinodimethane with two butoxycarbonyl groups in 85% yield. Subsequently, C4BA was prepared through the [2 + 4] cycloaddition reaction of C_{60} and in situ generated *o*-quinodimethane from R3 in 57% yield. Meanwhile, the similar ester-exchange reaction of R1 with ethanol was unsuccessful because monoexchanged compound could not be removed by the silica gel chromatography. Alternatively, the [2 + 2 + 2] cyclotrimerization reaction[34] using 1,5-hexadiyne and commercially available diethyl acetylenedicarboxylate afforded R4 in 61% yield. Afterward, R4 reacted with C_{60} to provide C2BA in 51% yield. Overall, the shorter alkyl chain length apparently caused lower solubility of the fullerene bis-adducts (C6BA > C4BA > C2BA).

The fullerene bis-adduct products were further subjected to preparative HPLC, equipped with a Buckyprep column using toluene as the eluent (Figure S2 in the Supporting Information). In the HPLC trace of C4BA, five peaks were observed in a ratio of 7:24:34:30:5, and each fraction was repeatedly collected. The structures of each fraction were characterized by ^{1}H NMR, ^{13}C NMR, high-resolution MS, and UV−vis absorption spectroscopy. They were assigned in the order of elution time as *trans*-1, *trans*-2, *trans*-3, *trans*-4+*e* (a mixture of *trans*-4 and *e*), and *cis*-2+*cis*-3 (a mixture of *cis*-2 and *cis*-3) isomers, respectively. Both *trans*-4+*e* and *cis*-2+*cis*-3 isomers could not be separated to the pure isomers and used as a mixture. Only *cis*-1 isomer could not be obtained probably due to the steric hindrance. It should be noted here that six peaks were detected in the C6BA separation procedure by HPLC, i.e., *trans*-4 and *e* isomers of C6BA could be separated.[21] On the other hand, in the HPLC chart of C2BA, no clearly resolved peaks could be found. The severe peak tailings prohibited the isolation of the C2BA regioisomers. These results suggest that the solubility of the fullerene bis-adducts decreases with shortening the alkyl chain length, making it difficult to separate the corresponding bis-adduct isomers.

Optical Properties. UV−vis absorption spectra of the fullerene bis-adducts were measured in *o*-dichlorobenzene (ODCB). C6BA, C4BA, and C2BA bis-adduct mixtures show almost identical absorption properties (Figure 2a). In addition, the characteristic absorption spectra of the C4BA isomers are consistent with those of the corresponding isomers of C6BA (Figure 2b−f).[22] These results corroborate that UV−vis absorption properties of the fullerene bis-adduct isomers mainly depend on the addition patterns but bear little relevance

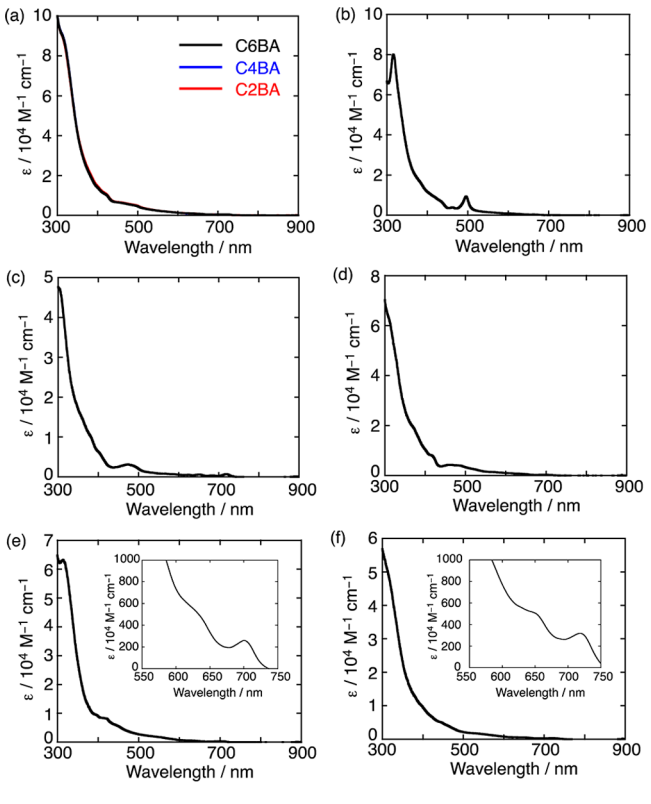

Figure 2. UV−vis absorption spectra of (a) C6BA (black), C4BA (blue), and C2BA (red) bis-adduct mixtures and (b) *trans*-1, (c) *trans*-2, (d) *trans*-3, (e) *trans*-4+*e* (mixture), (f) *cis*-2+*cis*-3 (mixture) isomers of C4BA in ODCB. The insets in (e) and (f) depict the enlarged absorption spectra from 550 to 750 nm.

to the alkyl chain length of substituents.[40−42] The spectrum of Figure 2e exhibits a weak band at 430 nm, which is characteristic of *e* isomer as reported in the literature.[40−42] Meanwhile, two broad bands at around 640 and 700 nm, typical of *trans*-4 isomer,[40−42] are observed as well (inset of Figure 2e). Thus, this fraction is certainly ascribed to a mixture of *trans*-4 and *e* isomers. Similarly, the spectrum in Figure 2f with a shoulder at 450 nm and small bands at 650 and 720 nm (inset of Figure 2f) results from both *cis*-2 and *cis*-3 isomers.

Electrochemical Properties and Theoretical Calculation. Electrochemical properties of the fullerene bis-adducts were investigated by cyclic voltammetry (CV) and differential pulse voltammetry (DPV) measurements (Figure 3). Table 1

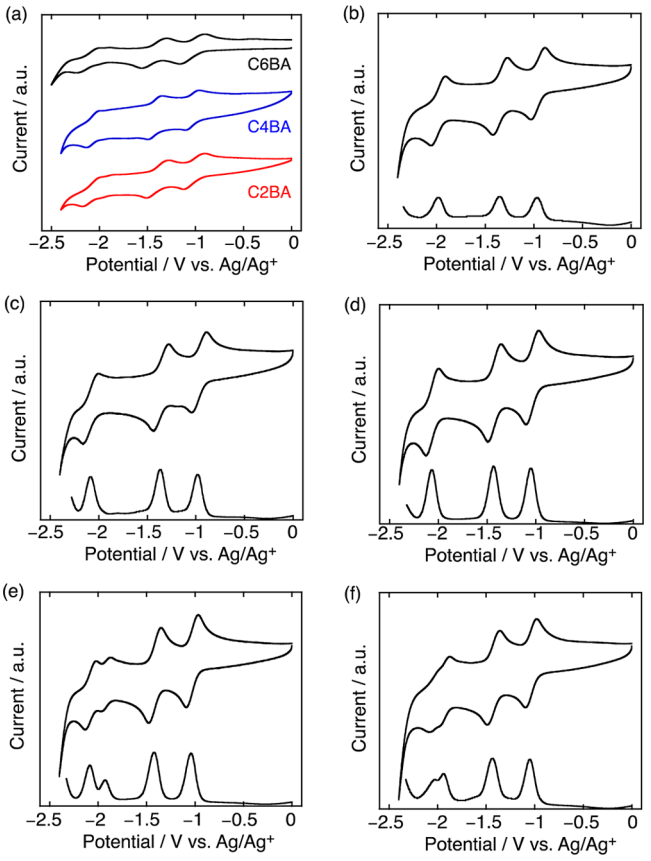

Figure 3. (a) Cyclic voltammograms of C6BA (upper), C4BA (middle), and C2BA (lower) bis-adduct mixtures and cyclic voltammograms (upper) and differential pulse voltammograms (lower) of (b) *trans*-1, (c) *trans*-2, (d) *trans*-3, (e) *trans*-4+*e* (mixture), and (f) *cis*-2+*cis*-3 (mixture) isomers of C4BA measured in ODCB/acetonitrile mixture (v:v = 5:1) containing 0.1 M tetrabutylammonium hexafluorophosphate (Bu_4PF_6). Sweep rate: 0.1 V s^{-1}; reference electrode, Ag/Ag^+ (0.01 M $AgNO_3$, 0.09 M Bu_4NPF_6 in acetonitrile).

lists the first (E_1), second (E_2), and third (E_3) reduction potentials determined by DPV measurements. Regioisomer mixtures of C6BA, C4BA, and C2BA exhibit three reversible reduction waves in the range from 0 to −2.5 V vs $Ag/AgNO_3$.[22] The reduction potentials are similar with deviations less than 0.03 V, which are within the limits of experimental error. Moreover, the reduction potentials of C4BA regioisomers are almost identical to those of C6BA isomers,[22] implying that the alkyl chain length of substituents on fullerene bis-adducts has little influence on their electrochemical properties. The LUMO energy levels of the fullerene bis-adducts, which are estimated

Table 1. Electrochemical Properties of Fullerene Bis-Adducts

fullerene	regioisomer	E_1/V[a]	E_2/V[a]	E_3/V[a]	LUMO/eV[b]
C6BA	mixture	−1.04	−1.42	−2.08	−3.67
C4BA	mixture	−1.05	−1.43	−2.08	−3.66
C2BA	mixture	−1.02	−1.40	−2.06	−3.69
C6BA	*trans*-1	−0.96	−1.35	−1.99	−3.75
C6BA	*trans*-2	−0.96	−1.35	−1.99	−3.75
C6BA	*trans*-3	−1.03	−1.42	−2.06	−3.68
C6BA	*trans*-4	−1.04	−1.44	−1.93	−3.67
C6BA	*e*	−1.02	−1.41	−2.08	−3.69
C6BA	*cis*-2+*cis*-3	−1.04	−1.43	−1.95	−3.67
C4BA	*trans*-1	−0.97	−1.35	−1.98	−3.74
C4BA	*trans*-2	−0.98	−1.37	−2.08	−3.73
C4BA	*trans*-3	−1.05	−1.44	−2.06	−3.66
C4BA	*trans*-4+*e*	−1.04	−1.42	−2.08	−3.67
C4BA	*cis*-2+*cis*-3	−1.05	−1.44	−2.03	−3.66
[60]PCBM	–	−0.90	−1.29	−1.99	−3.81

[a]Values are versus Ag/Ag^+. [b]$E_{LUMO} = -e(E_1 + 4.71)$ eV.

from the E_1 values,[43] are found to be 0.1−0.2 eV higher than [60]PCBM. This is beneficial for their application as an acceptor in PSC to improve V_{OC} values.

To get more insight into the electronic structures of fullerene bis-adduct isomers, we performed density functional theory (DFT) calculations using RB3LYP/6-31G (d) model. The methoxycarbonyl-substituted fullerene bis-adducts were used for simplicity, because the alkyl chains hardly have any impact on the electronic structures of fullerenes (vide supra). The LUMO levels were calculated after the geometry optimizations, as illustrated in Figure 4, and found to be largely consistent with the trend of experimental values. The electron densities of all the HOMOs and LUMOs of the fullerene bis-adduct isomers are primarily localized in the fullerene cores, but the distribution pattern of the electron densities varies with the regioisomers. It should be mentioned here, however, that Sabirov theoretically proved the critical importance of not only the LUMO levels but also the anisotropy of each isomer to determine the photovoltaic properties of respective solar cells in a recent report.[44]

Photovoltaic Properties. PSCs based on the ITO/PEDOT:PSS/P3HT:fullerene/Al configuration were fabricated to evaluate the photovoltaic performances of the fullerene bis-adducts. The detailed device-fabrication process is described in the Experimental Section. The averaged device parameters are summarized in Table 2. In the case of P3HT:[60]PCBM-based reference devices, a maximum PCE value reached up to 3.50% using the mixed solution of P3HT and [60]PCBM (1:0.6, w/w) in chlorobenzene (Figure S3 in the Supporting Information). However, C6BA, C4BA, and C2BA showed insufficient solubilities in chlorobenzene for the film formations by spin-coating. Accordingly, we used ODCB solutions for the device fabrications based on the fullerene bis-adducts for accurate comparison. The reference device based on P3HT:[60]PCBM was also fabricated using the ODCB solution. Note here that the weight ratio of [P3HT]:[CnBA mixture (n = 6, 4, 2) or [60]PCBM] was 1:0.9, which was previously optimized for the C6BA mixture-based device.[22]

The device based on the as-prepared C2BA bis-adduct mixture exhibits higher PCE value (1.20%) than those of the C4BA (1.10%) and C6BA (0.95%) isomer mixtures. Shortening the alkyl chain length causes a decrease in the solubility of the

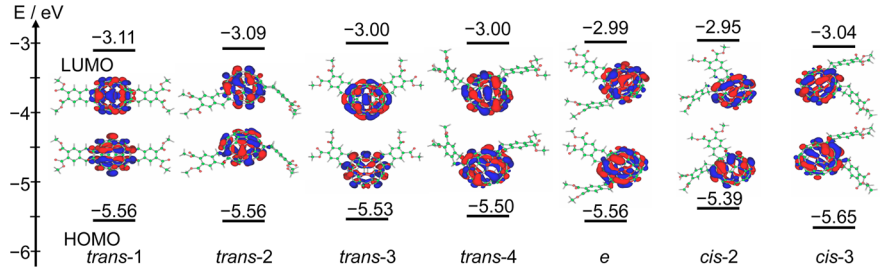

Figure 4. Optimized geometry, HOMO/LUMO electron density distribution, and energy levels of methoxycarbonyl-substituted fullerene bis-adduct isomers simulated by DFT calculations using RB3LYP/6-31G (d) model.

Table 2. Device Characteristics of Solar Cells Composed of P3HT and Fullerene Bis-Adducts or [60]PCBM under AM1.5 Conditions (100 mW cm^{-2})[a]

fullerene	regioisomer	weight ratio [P3HT]:[fullerene]	J_{SC}/mA cm^{-2}	V_{OC}/V	FF	PCE/%
C6BA	mixture	1:0.9	3.71 ± 0.05	0.677 ± 0.006	0.379 ± 0.031	0.95 ± 0.08
C4BA	mixture	1:0.9	5.05 ± 0.31	0.552 ± 0.002	0.394 ± 0.016	1.10 ± 0.12
C2BA	mixture	1:0.9	4.02 ± 0.19	0.574 ± 0.008	0.520 ± 0.027	1.20 ± 0.13
[60]PCBM[b]	–	1:0.9	6.77 ± 0.48	0.636 ± 0.008	0.487 ± 0.010	2.10 ± 0.38
C6BA	*trans*-1	1:0.9	1.43 ± 0.01	0.288 ± 0.078	0.295 ± 0.013	0.12 ± 0.03
C6BA	*trans*-2	1:0.9	4.73 ± 0.35	0.728 ± 0.006	0.402 ± 0.002	1.38 ± 0.07
C6BA	*trans*-3	1:0.9	3.57 ± 0.09	0.647 ± 0.058	0.387 ± 0.019	0.89 ± 0.13
C6BA	*trans*-4	1:0.9	4.63 ± 0.04	0.706 ± 0.002	0.440 ± 0.037	1.44 ± 0.13
C6BA	*e*	1:0.9	4.56 ± 0.12	0.699 ± 0.023	0.442 ± 0.030	1.41 ± 0.11
C6BA	*cis*-2+*cis*-3	1:0.9	3.44 ± 0.13	0.574 ± 0.001	0.312 ± 0.015	0.62 ± 0.06
C4BA	*trans*-1	1:0.7	3.22 ± 0.42	0.525 ± 0.014	0.321 ± 0.014	0.54 ± 0.10
C4BA	*trans*-2	1:0.7	6.82 ± 0.17	0.711 ± 0.033	0.497 ± 0.011	2.41 ± 0.13
C4BA	*trans*-3	1:0.7	5.61 ± 0.09	0.649 ± 0.020	0.399 ± 0.022	1.45 ± 0.10
C4BA	*trans*-4+*e*	1:0.7	6.84 ± 0.52	0.705 ± 0.026	0.488 ± 0.007	2.35 ± 0.23
C4BA	*cis*-2+*cis*-3	1:0.7	3.04 ± 0.19	0.452 ± 0.007	0.326 ± 0.007	0.45 ± 0.03
[60]PCBM[c]	–	1:0.6	8.77 ± 0.07	0.626 ± 0.003	0.637 ± 0.010	3.50 ± 0.05

[a]The photovoltaic parameters are average values from more than six independent experiments. [b]Reference device fabricated under the same conditions as other fullerene bis-adduct-based devices. [c]Device fabricated under the optimized conditions using chlorobenzene as the spin-coating solvent for the P3HT:[60]PCBM-based device.

bis-adducts in common organic solvents including toluene and ODCB, but an increase in the PCE values of the PSC devices (Table 2). The shorter insulating addends that surround the fullerene core may lead to an increase in the electron mobility and a reduction in series resistance, which stems from more close packing of the fullerene cores induced by the shorter alkyl chains. Different regioisomer distribution, i.e., 3:18:31:11:29:7 of *trans*-1:*trans*-2:*trans*-3:*trans*-4:*e*:*cis*-2+*cis*-3 (mixture) for C6BA[22] and 7:24:34:30:5 of *trans*-1: *trans*-2:*trans*-3:*trans*-4+*e* (mixture):*cis*-2+*cis*-3 (mixture) for C4BA, may also contribute to a switch order of some of the photovoltaic parameters. Note that the reference device based on P3HT:[60]PCBM shows a higher PCE value of 2.10%, with V_{OC} = 0.636 V, J_{SC} = 6.77 mA cm^{-2}, and FF = 0.487. Unexpectedly, the V_{OC} values of the devices with C4BA (0.552 V) and C2BA (0.574 V) were lower than that with [60]PCBM (0.636 V) despite the elevated LUMO energy level. The inferior V_{OC} values may be attributed to other factors such as more frequent occurrence of charge recombination in the P3HT:fullerene bis-adduct isomer films.

Although the C2BA mixture-based device showed a higher device performance than the C4BA and C6BA mixture-based ones, the regioisomers of C2BA could not be separated owing to the low solubility. Consequently, in the following part PSCs based on the C4BA and C6BA regioisomers are further dealt with to investigate the effects of alkyl chain length and substituent pattern of the fullerene bis-adducts on the film structures and photovoltaic properties. To optimize the weight ratio of [P3HT]:[C4BA isomer] for the photoactive layer, we changed the weight ratio from 1:0.6 to 1:1 by using C4BA–*trans*-2 as a representative isomer and found that the ratio of 1:0.7 yielded the best photovoltaic performance. The best weight ratio of C4BA–*trans*-2 is lower than that of C6BA isomers (1:0.9).[22] Due to the relatively low solubility of C4BA isomers, the high concentration may induce large aggregations and deteriorate the device performance. Thus, we used the weight ratio of 1:0.7 for the film formation of P3HT:C4BA isomers as the photoactive layers (Table 2). In both the series of C6BA and C4BA, the *trans*-2, *trans*-4, and *e* isomer-based solar cells reveal similar PCE values, which are significantly higher than those of *trans*-1, *trans*-3, *cis*-2, and *cis*-3 isomer-based solar cells (Table 2). Although the relationships between the LUMO levels and the resulting V_{OC} values are also unclear for the isomerically separated fullerene bis-adduct, the former devices exclusively achieved higher V_{OC} values (≥0.70 V) than [60]PCBM. In addition, the devices based on the C4BA regioisomers exhibited superior performance compared to those based on the corresponding C6BA regioisomers. The devices with *trans*-2 and *trans*-4+*e* isomers of C4BA as electron-acceptor materials exhibit PCEs of ca. 2.4%, which are increased by 70% compared to the corresponding regioisomers of C6BA (ca. 1.4%). Due to the limited availability of the samples with relatively large amounts, henceforth we decided to focus on *trans*-2 and *trans*-3 of C4BA and C6BA (denoted as C4BA–*trans*-2, C4BA–*trans*-3, C6BA–*trans*-2, and C6BA–*trans*-3) as

the contrasting representative examples. The current density–voltage characteristics and photocurrent action spectra of the devices with these four fullerene isomers are depicted in Figure 5.

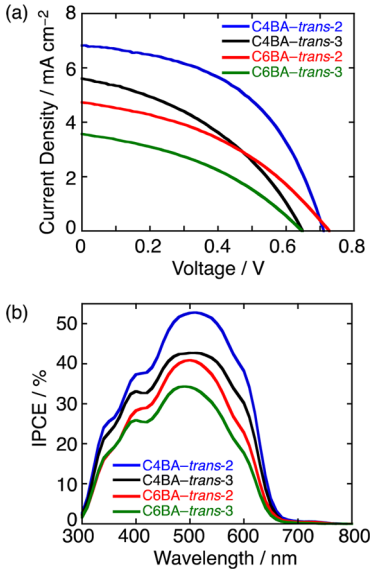

Figure 5. (a) Current density–voltage characteristics under illumination and (b) photocurrent action spectra of the PSC devices based on P3HT and fullerene isomers of C4BA–*trans*-2, C4BA–*trans*-3, C6BA–*trans*-2, and C6BA–*trans*-3.

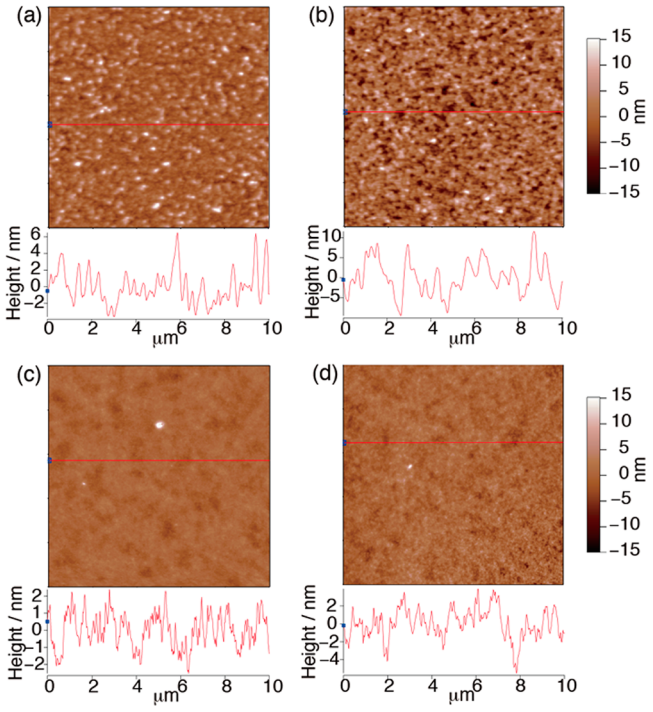

Figure 6. Tapping-mode atomic force micrographs of (a) P3HT:C4BA–*trans*-2, (b) P3HT:C4BA–*trans*-3, (c) P3HT:C6BA–*trans*-2, and (d) P3HT:C6BA–*trans*-3 films spin-coated on ITO/PEDOT:PSS substrate. The color scale represents the height topography, with bright and dark representing the highest and lowest features, respectively. The rms surface roughnesses are (a) 1.2, (b) 2.5, (c) 0.72, and (d) 0.74 nm, respectively.

Comparison of C4BA and C6BA. The large PCE values of C4BA–*trans*-2 and C4BA–*trans*-3-based devices mainly result from the enhanced J_{SC} values by ca. 50% relative to the devices based on the corresponding regioisomers of C6BA (Table 2 and Figure 5a). Consistently, the incident photon-to-current efficiency (IPCE) values of the devices with C4BA–*trans*-2 and C4BA–*trans*-3 are higher than those with C6BA–*trans*-2 and C6BA–*trans*-3 (Figure 5b).[45] These results suggest more efficient light-harvesting, charge separation, and charge transportation processes caused by the shorter alkyl chain substituents on the fullerene bis-adducts. Indeed, the absorptions of the P3HT:C4BA isomer films at peaks in the visible region (62%) are higher than those of P3HT:C6BA isomers (54%) by a factor of 1.15 (Figure S4, Supporting Information). It is noteworthy that the P3HT:C4BA isomers showed red-shifted absorption bands compared to the P3HT:C6BA isomers (Figure S4, Supporting Information), indicating the involvement of the fullerenes on the alignment of P3HT in the composite films.[46] The well-ordered polymer phase in the P3HT:C4BA isomer films may contribute to the relatively efficient hole transportation.

To shed light onto the relationship between the fullerene molecular structures, film structure of the P3HT:fullerene composite films, and device performances, surface morphologies of the P3HT:fullerene films were assessed by atomic force microscopy (AFM) measurements (Figure 6). The root-mean-square (rms) surface roughness values of the C4BA–*trans*-2 (1.2 nm) and C4BA–*trans*-3 (2.5 nm) films are larger than those of the C6BA–*trans*-2 (0.72 nm) and C6BA–*trans*-3 (0.74 m) films. The relatively large sizes of phase separations seem to be associated with the highly ordered structures of P3HT in the P3HT:C4BA isomer films. The shorter alkyl chain length of C4BA would decrease the miscibility with P3HT, resulting in larger phase separation of the polymer and fullerene derivative and in turn inhibition of the charge recombination. The degree of molecular ordering was further investigated by X-ray diffraction (XRD) analyses (Figure S5, Supporting Information). The C4BA isomer films show stronger diffraction intensity than the C6BA isomer films at 2θ = 5.23°, corresponding to the interchain spacing in P3HT associated with the interdigitated alkyl chains. The stronger XRD peaks imply the more ordered structure of P3HT aggregation in the composite films with C4BA isomers.

Comparison of *trans*-2 and *trans*-3 Isomers. The IPCE values of the C4BA–*trans*-2-based device exceed 50% in the wavelength range of 470–570 nm, which are higher than those of C4BA–*trans*-3-based device (Figure 5b), despite the analogous light-harvesting property of the two films (Figure S4, Supporting Information). This result suggests more efficient charge separation and charge transportation in the C4BA–*trans*-2-based device than the C4BA–*trans*-3-based one. Note here that AFM measurements reveal the rougher surface morphology of P3HT:C4BA–*trans*-3 than P3HT:C4BA–*trans*-2 (Figure 6). The domain growth would inhibit the undesirable charge recombination, but the photocurrent generation in BHJ solar cells could be limited by the reduced interfacial area between the fullerene- and polymer-rich domains. Thus, it can be speculated that the domain size in C4BA–*trans*-3 could become larger than the maximum exciton diffusion length (ca. 10 nm).[1−6] These arguments are consistent with the theoretical studies reported by Sabirov,[44] i.e., the lower anisotropy of polarizability of the *trans*-2 isomer of bis(dihydronaphtho)-fullerene than the *trans*-3 isomer would facilitate the miscibility

with P3HT in the BHJ films, leading to a decrease in the volume fraction of fullerene- and polymer-rich domains.

The same tendencies of the IPCE values and absorptions are observed in the devices based on the C6BA isomers (Figure 5b and Figure S4, Supporting Information). It should be stated here that micrometer-sized phase separation was observed for only the P3HT:C6BA–*trans*-3 blend film,[22] although the other areas exhibit the smooth morphology (Figure 6d). This is surprising because C6BA–*trans*-2,[22] C6BA–*trans*-3,[22] C4BA–*trans*-2, and C4BA–*trans*-3 have sufficient, similar thermal stability for the device fabrication procedures,[22] as revealed by TGA and DSC measurements (Figure S6 and Figure S7, Supporting Information). Although the reason for the large phase separation in P3HT:C6BA–*trans*-3 is unclear at the current stage, the high anisotropy of *trans*-3 isomer compared to *trans*-2 isomer and longer alkyl chain (hexyl vs butyl) may facilitate the aggregation of C6BA–*trans*-3 during the heat annealing. This micrometer-sized crystallization of fullerene phase would cause the reduction of interfacial area between the donor and the acceptor, thereby leading to the relatively low charge separation efficiency. Consistently, the photoluminescence spectra of P3HT with C4BA–*trans*-2, C4BA–*trans*-3, and C6BA–*trans*-2 reveal comparable quenching (84–85%) of the P3HT emission, which is more intense than that (65%) of the P3HT:C6BA–*trans*-3 film (Figure S8, Supporting Information). The unfavorable phase separation structure in the P3HT:C6BA–*trans*-3 film rationalizes the considerable decrease in J_{SC} (3.57 mA cm^{-2}) and PCE (0.89%) in comparison with the C6BA–*trans*-2-based device (J_{SC} of 4.73 mA cm^{-2} and PCE of 1.38%).[22]

Electron Mobility. Electron mobilities of the fullerene isomers were examined by the space-charge limited current (SCLC) method.[32,47] Dark current density–voltage curves of electron-only devices (Al/P3HT:fullerene isomer/Al) are displayed in Figure 7. The values of electron mobility are calculated from the following equation

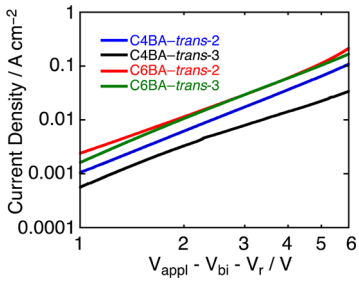

Figure 7. Current density–voltage characteristics in dark of electron-only devices based on P3HT and fullerene isomers of C4BA–*trans*-2, C4BA–*trans*-3, C6BA–*trans*-2, and C6BA–*trans*-3.

$$J = \frac{9}{8}\varepsilon_r\varepsilon_0\mu\frac{V^2}{d^3}$$

where J is the current density, ε_r is the dielectric constant of fullerene derivatives (3.5), ε_0 is the permittivity of vacuum (8.85×10^{-10} C V^{-1} cm^{-1}), μ is electron mobility, $V = V_{appl} - V_{bi} - V_r$, V_{appl} is the applied potential, V_{bi} is the built-in potential resulting from work function difference of two electrodes (in this device, V_{bi} = 0 V), V_r is the voltage drop due to the resistance, and d is film thickness. Electron mobilities obtained for the P3HT:C4BA–*trans*-2, P3HT:C4BA–*trans*-3, P3HT:C6BA–*trans*-2, and P3HT:C6BA–*trans*-3 blend films are 8.2×10^{-5}, 2.2×10^{-5}, 6.9×10^{-5}, and 5.5×10^{-5} cm^2 V^{-1} s^{-1}, respectively.[48] The P3HT:C4BA–*trans*-2 film having the best PSC device performance indeed exhibited the highest electron mobility. Additionally, *trans*-2 isomers show higher electron mobilities than the corresponding *trans*-3 isomers, implying a better-aligned structure of *trans*-2 isomers than *trans*-3 isomers. However, there are still discrepancies in the relationship between the electron mobilities and J_{SC} values in respective PSCs. These results indicate that the electron transport efficiency depends on the electron mobility as well as the phase separation structures in the composite films.

CONCLUSIONS

In summary, a series of alkoxycarbonyl-substituted dihydronaphthyl-based [60]fullerene bis-adduct derivatives (C2BA, C4BA, and C6BA with the alkyl chain of ethyl, *n*-butyl, and *n*-hexyl, respectively) have been synthesized through Diels–Alder reaction in moderate yields. The *trans*-1, *trans*-2, *trans*-3, *trans*-4+*e* (mixture), and *cis*-2+*cis*-3 (mixture) isomers of the C4BA products were isolated by preparative HPLC, although the isomers of C2BA could not be separated. The shorter alkyl chain length caused lower solubility of the fullerene bis-adducts (C6BA > C4BA > C2BA), making it difficult to separate respective bis-adduct isomer in the order. However, the alkyl chain length of the substituents on the fullerene bis-adducts had little impact on their optical and electrochemical properties. PSCs based on the P3HT:fullerene bis-adducts blend films were fabricated to evaluate the photovoltaic performance under the same optimized conditions. The device performance of fullerene bis-adducts was enhanced with the shortening of alkyl chain length. The devices based on *trans*-2, *trans*-4, and *e* isomers of C4BA exhibited similar PCE values of ca. 2.4%, which are increased by 70% relative to the C6BA counterparts (ca. 1.4%). There is no clear relationship between the PSC device performances and the LUMO energy levels of the fullerene regioisomers, whereas the film morphologies as well as electron mobilities of the P3HT:bis-adduct blend films unambiguously affect the photovoltaic properties. Such structure–photovoltaic performance relationship will provide valuable, basic information on the rational design of fullerene bis-adducts as an acceptor for highly efficient PSCs.

ASSOCIATED CONTENT

Supporting Information

Schematic illustrations for PSC devices (S1), HPLC profiles (S2), an *I*–*V* curve (S3), UV–vis absorption spectra (S4), XRD patterns (S5), TGA (S6), DSC (S7), and photoluminescence spectra (S8). This material is available free of charge via the Internet at http://pubs.acs.org.

AUTHOR INFORMATION

Corresponding Author

*E-mail: imahori@scl.kyoto-u.ac.jp. Fax: +81-75-383-2571. Tel: +81-75-383-2566.

Notes

The authors declare no competing financial interest.

ACKNOWLEDGMENTS

This work is supported by New Energy and Industrial Technology Development Organization (NEDO) and Grand-in-Aid (No. 25220801 to H.I.). The authors thank Micro/

NanoFabrication Hub (Kyoto University), Dr. Hisahi Yashiro, and Mr. Sin-ichi Sato (Rigaku) for XRD measurements.

REFERENCES

(1) Thompson, B. C.; Fréchet, J. M. J. Polymer−Fullerene Composite Solar Cells. *Angew. Chem., Int. Ed.* **2008**, *47*, 58−77.

(2) Cheng, Y.-J.; Yang, S.-H.; Hsu, C.-S. Synthesis of Conjugated Polymers for Organic Solar Cell Applications. *Chem. Rev.* **2009**, *109*, 5868−5923.

(3) Arias, A. C.; MacKenzie, J. D.; McCulloch, I.; Rivnay, J.; Salleo, A. Materials and Applications for Large Area Electronics: Solution-Based Approaches. *Chem. Rev.* **2010**, *110*, 3−24.

(4) Li, G.; Zhu, R.; Yang, Y. Polymer Solar Cells. *Nat. Photonics* **2012**, *6*, 153−161.

(5) Li, Y. F. Molecular Design of Photovoltaic Materials for Polymer Solar Cells: Toward Suitable Electronic Energy Levels and Broad Absorption. *Acc. Chem. Res.* **2012**, *45*, 723−733.

(6) Umeyama, T.; Imahori, H. Design and Control of Organic Semiconductors and Their Nanostructures for Polymer−Fullerene-Based Photovoltaic Devices. *J. Mater. Chem. A* **2014**, *2*, 11545−11560.

(7) He, Z. C.; Zhong, C. M.; Su, S. J.; Xu, M.; Wu, H. B.; Cao, Y. Enhanced Power-Conversion Efficiency in Polymer Solar Cells Using an Inverted Device Structure. *Nat. Photonics* **2012**, *6*, 591−595.

(8) Scharber, M. S.; Mühlbacher, D.; Koppe, M.; Denk, P.; Waldauf, C.; Heeger, A. J.; Brabec, C. J. Design Rules for Donors in Bulk-Heterojunction Solar Cells−Towards 10% Energy-Conversion Efficiency. *Adv. Mater.* **2006**, *18*, 789−794.

(9) Qi, B.; Wang, J. Open-Circuit Voltage in Organic Solar Cells. *J. Mater. Chem.* **2012**, *22*, 24315−24325.

(10) Lenes, M.; Wetzelaer, G.-J. A. H.; Kooistra, F. B.; Veenstra, S. C.; Hummelen, J. C.; Blom, P. W. M. Fullerene Bisadducts for Enhanced Open-Circuit Voltages and Efficiencies in Polymer Solar Cells. *Adv. Mater.* **2008**, *20*, 2116−2119.

(11) Lenes, M.; Shelton, S. W.; Sieval, A. B.; Kronholm, D. F.; Hummelen, J. C.; Blom, P. W. M. Electron Trapping in Higher Adduct Fullerene-Based Solar Cells. *Adv. Funct. Mater.* **2009**, *19*, 3002−3007.

(12) Dyer-Smith, C.; Reynolds, L. X.; Bruno, A.; Bradley, D. D. C.; Haque, S. A.; Nelson, J. Triplet Formation in Fullerene Multi-Adduct Blends for Organic Solar Cells and Its Influence on Device Performance. *Adv. Funct. Mater.* **2010**, *20*, 2701−2708.

(13) He, Y.; Chen, H.-Y.; Hou, J.; Li, Y. Indene-C_{60} Bisadduct: A New Acceptor for High-Performance Polymer Solar Cells. *J. Am. Chem. Soc.* **2010**, *132*, 1377−1382.

(14) Zhao, G.; He, Y.; Li, Y. 6.5% Efficiency of Polymer Solar Cells Based on Poly(3-hexylthiophene) and Indene-C_{60} Bisadduct by Device Optimization. *Adv. Mater.* **2010**, *22*, 4355−4358.

(15) He, Y.; Zhao, G.; Peng, B.; Li, Y. High-Yield Synthesis and Electrochemical and Photovoltaic Properties of Indene-C_{70} Bisadduct. *Adv. Funct. Mater.* **2010**, *20*, 3383−3389.

(16) Cheng, Y.-J.; Liao, M.-H.; Chang, C.-Y.; Kao, W.-S.; Wu, C.-E.; Hsu, C.-S. Di(4-methylphenyl)methano-C_{60} Bis-Adduct for Efficient and Stable Organic Photovoltaics with Enhanced Open-Circuit Voltage. *Chem. Mater.* **2011**, *23*, 4056−4062.

(17) He, Y.; Peng, B.; Zhao, G.; Zou, Y.; Li, Y. Indene Addition of 6,6-Phenyl-C_{61}-butyric Acid Methyl Ester for High-Performance Acceptor in Polymer Solar Cells. *J. Phys. Chem. C* **2011**, *115*, 4340−4344.

(18) Kim, K.-H.; Kang, H.; So Yeon, N.; Jung, J.; Kim, P. S.; Cho, C.-H.; Lee, C.; Yoon, S. C.; Kim, B. J. Facile Synthesis of *o*-Xylenyl Fullerene Multiadducts for High Open Circuit Voltage and Efficient Polymer Solar Cells. *Chem. Mater.* **2011**, *23*, 5090−5095.

(19) Li, C.-Z.; Chien, S.-C.; Yip, H.-L.; Chueh, C.-C.; Chen, F.-C.; Matsuo, Y.; Nakamura, E.; Jen, A. K. Y. Facile Synthesis of a 56 π-Electron 1,2-Dihydromethano-[60]PCBM and Its Application for Thermally Stable Polymer Solar Cells. *Chem. Commun.* **2011**, *47*, 10082−10084.

(20) Deng, L.-L.; Feng, J.; Sun, L.-C.; Wang, S.; Xie, S.-L.; Xie, S.-Y.; Huang, R.-B.; Zheng, L.-S. Functionalized Dihydronaphthyl-C_{60} Derivatives as Acceptors for Efficient Polymer Solar Cells with Tunable Photovoltaic Properties. *Sol. Energy Mater. Sol. Cells* **2012**, *104*, 113−120.

(21) He, Y.; Chen, C.; Richard, E.; Dou, L.; Wu, Y.; Li, G.; Yang, Y. Novel Fullerene Acceptors: Synthesis and Application in Low Band Gap Polymer Solar Cells. *J. Mater. Chem.* **2012**, *22*, 13391−13394.

(22) Kitaura, S.; Kurotobi, K.; Sato, M.; Takano, Y.; Umeyama, T.; Imahori, H. Effects of Dihydronaphthyl-Based [60]fullerene Bisadduct Regioisomers on Polymer Solar Cell Performance. *Chem. Commun.* **2012**, *48*, 8550−8552.

(23) Meng, X.; Zhang, W.; Tan, Z. a.; Du, C.; Li, C.; Bo, Z.; Li, Y.; Yang, X.; Zhen, M.; Jiang, F.; Zheng, J.; Wang, T.; Jiang, L.; Shu, C.; Wang, C. Dihydronaphthyl-Based [60]Fullerene Bisadducts for Efficient and Stable Polymer Solar Cells. *Chem. Commun.* **2012**, *48*, 425−427.

(24) Meng, X.; Zhang, W.; Tan, Z. a.; Li, Y.; Ma, Y.; Wang, T.; Jiang, L.; Shu, C.; Wang, C. Highly Efficient and Thermally Stable Polymer Solar Cells with Dihydronaphthyl-Based [70]Fullerene Bisadduct Derivative as the Acceptor. *Adv. Funct. Mater.* **2012**, *22*, 2187−2193.

(25) Zhang, C. Y.; Chen, S.; Xiao, Z.; Zuo, Q. Q.; Ding, L. M. Synthesis of Mono- and Bisadducts of Thieno-*o*-quinodimethane with C_{60} for Efficient Polymer Solar Cells. *Org. Lett.* **2012**, *14*, 1508−1511.

(26) Ye, L.; Zhang, S.; Qian, D.; Wang, Q.; Hou, J. Application of Bis-PCBM in Polymer Solar Cells with Improved Voltage. *J. Phys. Chem. C* **2013**, *117*, 25360−25366.

(27) He, Y.; Li, Y. Fullerene Derivative Acceptors for High Performance Polymer Solar Cells. *Phys. Chem. Chem. Phys.* **2011**, *13*, 1970−1983.

(28) Li, Y. F. Fullerene-Bisadduct Acceptors for Polymer Solar Cells. *Chem.—Asian J.* **2013**, *8*, 2316−2328.

(29) Nardes, A. M.; Ferguson, A. J.; Whitaker, J. B.; Larson, B. W.; Larsen, R. E.; Maturová, K.; Graf, P. A.; Boltalina, O. V.; Strauss, S. H.; Kopidakis, N. Beyond PCBM: Understanding the Photovoltaic Performance of Blends of Indene-C_{60} Multiadducts with Poly(3-hexylthiophene). *Adv. Funct. Mater.* **2012**, *22*, 4115−4127.

(30) Xiao, Z.; Matsuo, Y.; Soga, I.; Nakamura, E. Structurally Defined High-LUMO-Level 66π-[70]Fullerene Derivatives: Synthesis and Application in Organic Photovoltaic Cells. *Chem. Mater.* **2012**, *24*, 2572−2582.

(31) Liao, M.-H.; Lai, Y.-Y.; Lai, Y.-Y.; Chen, Y.-T.; Tsai, C.-E.; Liang, W.-W.; Cheng, Y.-J. Reducing Regioisomers of Fullerene-Bisadducts by Tether-Directed Remote Functionalization: Investigation of Electronically and Sterically Isomeric Effects on Bulk-Heterojunction Solar Cells. *ACS Appl. Mater. Interfaces* **2013**, *6*, 996−1004.

(32) Meng, X. Y.; Xu, Q.; Zhang, W. Q.; Tan, Z. A.; Li, Y. F.; Zhang, Z. X.; Jiang, L.; Shu, C. Y.; Wang, C. R. Effects of Alkoxy Chain Length in Alkoxy-Substituted Dihydronaphthyl-Based [60]Fullerene Bisadduct Acceptors on Their Photovoltaic Properties. *ACS Appl. Mater. Interfaces* **2012**, *4*, 5966−5973.

(33) Meng, X.; Zhao, G.; Xu, Q.; Tan, Z. a.; Zhang, Z.; Jiang, L.; Shu, C.; Wang, C.; Li, Y. Effects of Fullerene Bisadduct Regioisomers on Photovoltaic Performance. *Adv. Funct. Mater.* **2014**, *24*, 158−163.

(34) Kotha, S.; Khedkar, P. Differential Reactivity Pattern of Hybrid *o*-Quinodimethane Precursors: Strategic Expansion to Annulated Benzocycloalkanes via Rongalite. *J. Org. Chem.* **2009**, *74*, 5667−5670.

(35) Frisch, M. J.; Trucks, G. W.; Schlegel, H. B.; Scuseria, G. E.; Robb, M. A.; Cheeseman, J. R.; Montgomery, J. A., Jr.; Vreven, T.; Kudin, K. N.; Burant, J. C.; Millam, J. M.; Iyengar, S. S.; Tomasi, J.; Barone, V.; Mennucci, B.; Cossi, M.; Scalmani, G.; Rega, N.; Petersson, G. A.; Nakatsuji, H.; Hada, M.; Ehara, M.; Toyota, K.; Fukuda, R.; Hasegawa, J.; Ishida, M.; Nakajima, T.; Honda, Y.; Kitao, O.; Nakai, H.; Klene, M.; Li, X.; Knox, J. E.; Hratchian, H. P.; Cross, J. B.; Bakken, V.; Adamo, C.; Jaramillo, J.; Gomperts, R.; Stratmann, R. E.; Yazyev, O.; Austin, A. J.; Cammi, R.; Pomelli, C.; Ochterski, J. W.; Ayala, P. Y.; Morokuma, K.; Voth, G. A.; Salvador, P.; Dannenberg, J. J.; Zakrzewski, V. G. ; Dapprich, S.; Daniels, A. D.; Strain, M. C.; Farkas, O.; Malick, D. K.; Rabuck, A. D.; Raghavachari, K.; Foresman, J. B.; Ortiz, J. V.; Cui, Q.; Baboul, A. G.; Clifford, S.; Cioslowski, J.; Stefanov, B. B.; Liu, G.; Liashenko, A.; Piskorz, P.; Komaromi, I.; Martin, R. L.; Fox, D. J.; Keith, T.; Al.Laham, M. A.; Peng, C. Y.;

Nanayakkara, A.; Challacombe, M.; Gill, P. M. W.; Johnson, B.; Chen, W.; Wong, M. W.; Gonzalez, C.; Pople, J. A. *Gaussian 03*; Gaussian, Inc.: Wallingford, CT, 2004.

(36) Umeyama, T.; Takamatsu, T.; Tezuka, N.; Matano, Y.; Araki, Y.; Yoshikawa, O.; Sagawa, T.; Yoshikawa, S.; Imahori, H. Synthesis and Photophysical and Photovoltaic Properties of Porphyrin-Furan and -Thiophene Alternating Copolymers. *J. Phys. Chem. C* **2009**, *113*, 10819−10828.

(37) Umeyama, T.; Hirose, K.; Noda, K.; Matsushige, K.; Shishido, T.; Saarenpää, H.; Tkachenko, N. V.; Lemmetyinen, H.; Ono, N.; Imahori, H. Donor−Acceptor Alternating Copolymer Based on Thermally Converted Isothianaphthene Dimer and Thiazolothiazole Subunits. *J. Phys. Chem. C* **2012**, *116*, 17414−17423.

(38) Umeyama, T.; Watanabe, Y.; Oodoi, M.; Evgenia, D.; Shishido, T.; Imahori, H. Synthesis of Low Bandgap Polymers Based on Thienoquinodimethane Units and Their Applications in Bulk Heterojunction Solar Cells. *J. Mater. Chem.* **2012**, *22*, 24394−24402.

(39) Umeyama, T.; Watanabe, Y.; Evgenia, D.; Imahori, H. Effect of Fluorine Substitution on Photovoltaic Properties of Benzothiadiazole−Carbazole Alternating Copolymers. *J. Phys. Chem. C* **2013**, *117*, 21148−21157.

(40) Nakamura, Y.; O-Kawa, K.; Matsumoto, M.; Nishimura, J. Separation and Characterization of [60]Fullerene Bisadducts Modified by 4,5-Dimethoxy-*o*-quinodimethane. *Tetrahedron* **2000**, *56*, 5429−5434.

(41) Kordatos, K.; Bosi, S.; Ros, T. D.; Zambon, A.; Lucchini, V.; Prato, M. Isolation and Characterization of All Eight Bisadducts of Fulleropyrrolidine Derivatives. *J. Org. Chem.* **2001**, *66*, 2802−2808.

(42) Nakamura, Y.; Takano, N.; Nishimura, T.; Yashima, E.; Sato, M.; Kudo, T.; Nishimura, J. First Isolation and Characterization of Eight Regioisomers for [60]Fullerene−Benzyne Bisadducts. *Org. Lett.* **2001**, *3*, 1193−1196.

(43) Although LUMO levels of C6BA isomers were estimated from reduction onsets in the previous report,[22] we herein employ E_1 values determined from DPV measurements where the potentials can be determined accurately. Larson, B. W.; Whitaker, J. B.; Wang, X.-B.; Popov, A. A.; Rumbles, G.; Kopidakis, N.; Strauss, S. H.; Boltalina, O. V. Electron Affinity of Phenyl−C_{61}−Butyric Acid Methyl Ester (PCBM). *J. Phys. Chem. C* **2013**, *117*, 14958−14964.

(44) Sabirov, D. S. Anisotropy of Polarizability of Fullerene Higher Adducts for Assessing the Efficiency of Their Use in Organic Solar Cells. *J. Phys. Chem. C* **2013**, *117*, 9148−9153.

(45) The J_{SC} values calculated by convolution of the spectral response with the photon flux of the AM 1.5G spectrum for the C4BA−*trans*-2, C4BA−*trans*-3, C6BA−*trans*-2, and C6BA−*trans*-3-based devices are 6.9, 5.6, 4.9, and 3.7 mA cm^{-2}, respectively. Because of the discrepancy between the IPCE results and the photon flux under AM 1.5 illumination, a mismatch of less than 4% was present between the convolution and the solar simulator spectra.

(46) Blom, P. W. M.; Mihailetchi, V. D.; Koster, L. J. A.; Markov, D. E. Device Physics of Polymer:Fullerene Bulk Heterojunction Solar Cells. *Adv. Mater.* **2007**, *19*, 1551−1566.

(47) Zhao, G.; He, Y.; Xu, Z.; Hou, J.; Zhang, M.; Min, J.; Chen, H.-Y.; Ye, M.; Hong, Z.; Yang, Y.; Li, Y. Effect of Carbon Chain Length in the Substituent of PCBM-like Molecules on Their Photovoltaic Properties. *Adv. Funct. Mater.* **2010**, *20*, 1480−1487.

(48) The electron mobility for P3HT:[60]PCBM blend film (1.3×10^{-4} cm^2 V^{-1} s^{-1}) fabricated under the same condition is close to the reported value,[32] supporting the validity of our measurements.